Turbulence enhancement in body force opposed flows

S. Jackson and S. He*
Department of Mechanical Engineering, University of Sheffield, Sheffield, S1 3JD, United Kingdom

(Received 2 June 2023; accepted 1 February 2024; published 5 March 2024)

Turbulence may be strongly influenced by near-wall nonuniform body forces. A widely encountered example is buoyancy acting in mixed convection flows. Here we use direct numerical simulations to present two key ideas: First we show that introducing opposing body forces whilst maintaining the pressure gradient does not cause key turbulence characteristics to change. It follows that the concept of "apparent Reynolds number" introduced by He *et al.* [J. Fluid Mech. **809**, 31 (2016)] to explain laminarization can now be extended to explain the opposite phenomena of turbulence enhancement by opposing body forces. This new understanding has allowed turbulent shear stress and skin friction to be easily predicted simply from the nonuniform body force profile and reference data despite the nonequilibrium nature of the flow. Second, we analyze the flow in the context of turbulence regeneration cycle and provide evidence that complements the recent study from Jiménez [J. Fluid Mech. **945**, R3 (2022)], which suggests that streaks are more decoupled from the regeneration cycle than previously thought.

DOI: 10.1103/PhysRevFluids.9.034601

I. INTRODUCTION

The use of nonuniform streamwise body forces, while initially seeming abstract, is a useful generalization since it can underpin various physical phenomena. For example, Kühnen *et al.* [1], Scarselli *et al.* [2], and Kühnen *et al.* [3] studied flow control methods such as near-wall streamwise fluid injection, outer region baffles, and moving walls in order to flatten the velocity profile causing laminarization. The principle effect of all these control measures can be represented by adding a nonuniform body force, that is, they are seen as pseudobody forces. Xu *et al.* [4] investigated a radial sinewave body force to mimic bubble injection. Other examples of pseudobody forces occur in shear thinning and shear thickening fluids where a modified effective viscosity results in an additional viscous shear stress acting like aiding and opposing nonuniform body forces, respectively [5]. Physical body forces occur frequently in magnetohydrodynamics; for example, Henoch and Stace [6] apply both streamwise aiding and opposing lorentz forces to boundary layers to investigate the effect on drag, boundary layer thickness, and delaying transition. Finally, a key example for this paper is mixed convection flows where buoyancy may predominantly act as a nonuniform body force.

The key behaviors of turbulence in such flows can be conveniently outlined considering buoyancy-influenced flows even though the understanding is applicable to other flows. In a buoyancy aided flow (e.g., heated upward flow or cooled downward flow), the near wall streamwise velocity

*s.he@sheffield.ac.uk

increases, leading to a flattening of the velocity profile, whilst the turbulent shear stress profiles decreases toward zero as the flow laminarizes [7–12]. This has been shown to drastically reduce turbulent mixing and therefore heat transfer. Further increasing buoyancy leads to an inflectional, M-shaped velocity profile inducing flow instabilities, thus causing a regeneration of turbulence. For buoyancy opposed flow (e.g., heated downward flow or cooled upward flow) [13–15], heat transfer increases monotonically with stronger buoyancy as the velocity gradient increases near the wall and the turbulence shear stress increases (see Jackson *et al.* [7] for an early review of buoyancy aiding and opposed flows in mixed convection). There are two ways that buoyancy can affect turbulence, as shown by Petukhov and Polyakov [16]. The first is known as the "external" or "indirect" effect where buoyancy due to a mean density profile will change the mean velocity profile, leading to a change in turbulence production. The second "structural" or "direct" effect is from density fluctuations directly interacting with velocity fluctuations, stabilizing or destabilizing turbulence depending on the direction of the buoyancy. It is known that the indirect effect has a dominant effect in causing laminarization of turbulence in a vertical flow. An explanation of such indirect effects was given by Hall and Jackson [17], who proposed that the buoyancy causes a redistribution of the shear stress, and in the buoyancy aided case the shear stress may be reduced to zero in the near-wall region which causes strong laminarization whilst the shear is increased in the buoyancy opposed case leading to stronger turbulence. These changes are considered complex and difficult to model owing to their nonequilibrium nature, which is to say that properties do not obey the self-similarity based on either inner or outer scalings.

Recently He *et al.* [18] developed a new understanding of strongly laminarized flows by studying some idealized body forces using direct numerical simulation (DNS). It was demonstrated that, while the body force causes the flow to laminarize in comparison with the flow of an equal flow rate (EFR), the main turbulence characteristics are not reduced by such body forces relative to an equal pressure gradient (EPG) flow. By extension, the conventional laminarization is explained by a smaller "apparent Reynolds number" defined by the corresponding EPG flow. A similar result, but from the opposite perspective, is found by García and Alvariño [19], suggesting that decreasing the pressure gradient whilst maintaining the Reynolds number is sufficient to cause laminarization. A further extension of the apparent Reynolds number theory was given by He *et al.* [20] for laminarization in a buoyancy aided supercritical thermal flow. It was shown that property variations and the effects from inertia can all be considered as pseudobody forces, and that the combination of these body forces act to reduce the apparent Reynolds number of the flow. The theory shows very good predictions of turbulence shear stress and velocity profiles in comparison with the DNS reference data. Marensi *et al.* [21] found that this theory agrees well with linear stability analysis for heated upward flow of air and they further demonstrate the theory accurately predicts the region of transition/reverse transition in strong buoyancy influenced flows.

The question we address in this article is: can the apparent Reynolds number theory be extended to explain body force induced turbulence enhancement, and if so, to what extent can the theory predict the flow behaviors. Second, in light of the new understanding on such nonequilibrium turbulence, we discuss the roles that low-speed streaks play in the turbulence regeneration cycle. We provide complementary evidence to recent work by Jiménez [22] for channel flows, and Wu *et al.* [23] for boundary layers that streaks are more decoupled from the regeneration cycle than previously thought. Despite not being the focus, this work also contributes to the scaling and prediction of nonequilibrium turbulent flows. Previously, Coleman *et al.* [24] and Huang *et al.* [25] extended the Van Driest [26] scaling to consider heated flows, and Trettel and Larsson [27], and Patel *et al.* [28], to further account for flows with strong variations of thermal properties. Pecnik and Patel [29] derived and demonstrated the success of a so-called semilocal scaled transport equation for turbulence kinetic energy based on semilocal parameters and Van Driest velocity for heated flows. Through new scaling, these authors correlate the different fluid property effects (and hence, to some extent, explain these effects as similar to each other). All the above work considered flows without buoyancy (that is, forced convection only). We consider more complex, body force opposed flows and demonstrate that the new scaling "+1" achieves a similar result.

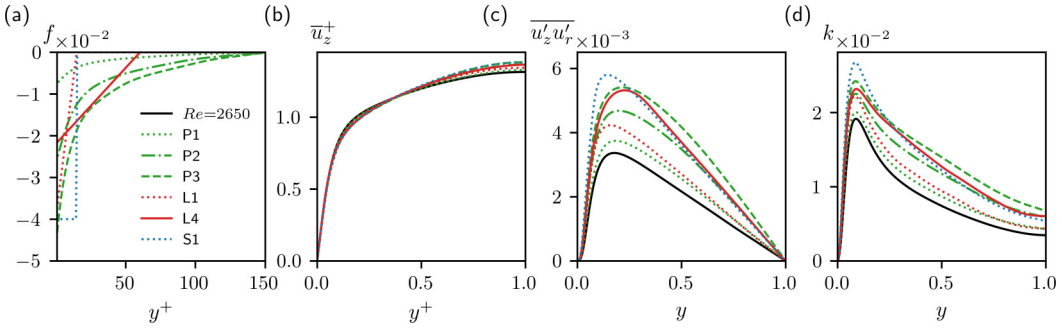

FIG. 1. Profiles of flow statistics for a selection of key cases: (a) body force profiles, (b) velocity profiles, (c) turbulence shear stress, and (d) turbulence kinetic energy.

II. METHODOLOGY

In this work, we apply a prescribed near wall nonuniform body force to an incompressible pipe flow, and study the influence on turbulence. First, we take the three downward turbulent flow cases from You *et al.* [30] and extract the profiles of buoyancy from their temperature profiles, which form cases P1–P3. Second, we create two sets of idealized profiles with systematically varying parameters. The first set, L1–L4 are linear profiles where L1 and L2 vary wall-normal coverage (y_c), while L3 and L4 vary body force strength at the wall (f_c). These are idealised profiles loosely designed to represent subcritical mixed convection. The second set S1, S2 are step change profiles with varying coverage designed to capture the sharp change in buoyancy which occurs at supercritical conditions [18]. We also include some aiding body force cases L1a, L2a, L3a which are useful for discussion in Sec. III C. Cases are run at a fixed mass flow rate with Reynolds number $Re_b = 2650$ with body force profiles illustrated in Fig. 1(a) and detailed in Table I. As mentioned in Sec. I, buoyancy causes changes in turbulence due to a structural effect and an external or indirect effect [16]. In a vertical flow, the latter is generally much stronger than the former, which is not accounted for in this isothermal flow representation. The momentum equations with the nonuniform body force hence reads

$$\frac{\partial u}{\partial t} + u \cdot \nabla u = -\nabla p + \frac{1}{Re}\nabla^2 u + f. \tag{1}$$

TABLE I. DNS cases for linear (L), step (S), and physical (P) body forces. All cases are opposing body force flows except those in parentheses which are aiding body force flows. L1 and L2 vary coverage, while L3 and L4 vary body force amplitude at the wall. For all cases $Re_b (= \frac{U_b R}{\nu}) = 2650$.

Case	Δ_z^+	$\Delta(r\theta)^+_{\max}$	$\Delta r^+_{\max}$	$\Delta r^+_{\min}$	$Re_{\tau p}$	Re_τ	y_c	f_c	$\lvert F \rvert$
EFR	6	4.7	4.9	0.11	180	180	–	–	–
L1 *(L1a)*	5.6 *(6.5)*	4.4 *(5.1)*	4.6 *(2.5)*	0.11 *(0.18)*	201 *(160)*	169 *(194)*	0.09	$-(+)0.04$	0.0035
L2 *(L2a)*	5.8 *(6.4)*	4.6 *(5.0)*	4.8 *(2.5)*	0.11 *(0.18)*	229 *(120)*	174 *(191)*	0.17	$-(+)0.04$	0.0063
L3 *(L3a)*	6.1 *(5.8)*	4.8 *(4.6)*	5.0 *(4.8)*	0.11 *(0.11)*	207 *(142)*	182 *(175)*	0.33	$-(+)0.01$	0.003
L4	6.1	4.8	5.0	0.12	235	181	0.33	-0.022	0.0065
S1	5.8	4.5	4.7	0.11	231	173	0.09	-0.04	0.0066
S2	6.1	4.8	3.0	0.07	277	182	0.17	-0.04	0.0126
P1-P3	5.8–6.0	4.6–4.7	5.8–5.9	0.13–0.14	188–217	175–180	–	–	0.002–0.011

The equation is nondimensionalized using the radius R^*, bulk velocity U_b^*, density ρ^*, and viscosity μ^* so that $Re = \frac{\rho^* U_b^* R^*}{\mu^*}$, $f = \frac{f^* R^*}{\rho^* U_b^{*2}}$, $p = \frac{p^*}{\rho^* U_b^{*2}}$. The DNSs are conducted using the Fortran code CHAPSim which uses a fractional step method with a second order central difference scheme for the spatial discretization [31,32]. The temporal terms are discretised with an explicit third order Runge-Kutta scheme for the nonlinear terms, and an implicit Crank-Nicholson scheme for the linear terms. All cases use a pipe flow domain of length $20R^*$, and in order to determine the strength of each body force profile, we use the integral $F = 2\int_0^1 rf\,dr$, as shown in Table I; we also often make use of the wall normal distance defined $y = 1 - r$. For large coverage cases (P1–P3) we note that the body forces extend beyond $y^+ = 60$ where the near wall regeneration cycle is most active [33]. We have found that the nonuniformity outside this region does not have a nonuniform impact on the flow, but rather is the same as adding an equivalent uniform (pressure) force. We hence shift the zero of the nonuniform force f to $y^+ = 60$ and modify the pressure term accordingly, that is, the modified body force $\hat{f} = f - f_{60}$ and pressure gradient $-\frac{\widehat{dp}}{dx} = -\frac{dp}{dx} + f_{60}$ where $f_{60} = f(y^+ = 60)$.

III. RESULTS

A. Physical description

The phenomenon we aim to explain is opposing body force induced turbulence enhancement. We begin by summarizing the precise changes to turbulent characteristics in such flows, and by methodically varying body force profile coverage and amplitude we show the effect of different body force profiles. The velocity profiles [Fig. 1(b)] change mildly, with increasing centerline velocity and reduced near wall velocity with the exception of very low coverage cases such as L1. Turbulence shear stress in Fig. 1(c) and turbulence kinetic energy in Fig. 1(d) show strong increases with increasing body force strength, in line with previous studies. It is interesting to note that the body force profile has a weaker effect. Comparing cases S1 and L4, which have similar body force strength, F, but very different profiles, it is clear that while there is a slight change in wall normal distribution of turbulence shear stress and turbulence kinetic energy, the overall turbulence enhancement is very similar between the two cases. In other words, the body force strength, F, provides a good indication of turbulence enhancement, whereas a change in the body force profile mostly causes a change in the wall normal distribution of turbulence.

B. Apparent Reynolds number theory

Figures 1(c) and 1(d) show a well-established phenomenon, that is, turbulence may be significantly enhanced by an opposing body force. This statement is based on comparing flows of the same flow rate. We ask what happens if one compares flows with/without nonuniform body forces or with different profiles but the same pressure gradient? Herein, we demonstrate that imposing a nonuniform body force causes no significant changes to turbulence when pressure gradient of the flow is kept unchanged (and hence, the total flow rate may reduce significantly). For simplicity, we introduce an equal flow rate (EFR) reference flow (used in conventional framework), and a new equal pressure pradient (EPG) reference flow. Referring to Eq. 1, a body force influenced flow is defined by its pressure gradient $\frac{dp}{dx}$, and body force f, whilst its EPG flow is due to an equal pressure gradient, that is, $\frac{dp}{dx}_{\text{EPG}} = \frac{dp}{dx}$, but has no body force ($f = 0$). This method leads to a new scaling whereby the wall shear stress of the EPG flow τ_{wp} is used as opposed to the standard wall shear stress of the body force influenced flow. This is denoted using a "+1" notation such that $y^{+1} = \frac{y u_{\tau p}}{\nu}$ and the Reynolds number of the EPG flow, $Re_{\tau p} = \frac{u_{\tau p} R}{\nu}$, is referred to as the apparent Reynolds number of the original body force influenced flow (here the friction velocity of the EPG flow is $u_{\tau p} = \sqrt{\frac{\tau_{wp}}{\rho}}$). All cases here can be compared under the EFR framework, however, an interesting thing to note is that the pair of cases L1 and L3, and also L2 and L4, have very similar $Re_{\tau p}$ and so those cases can also be considered together under the EPG framework.

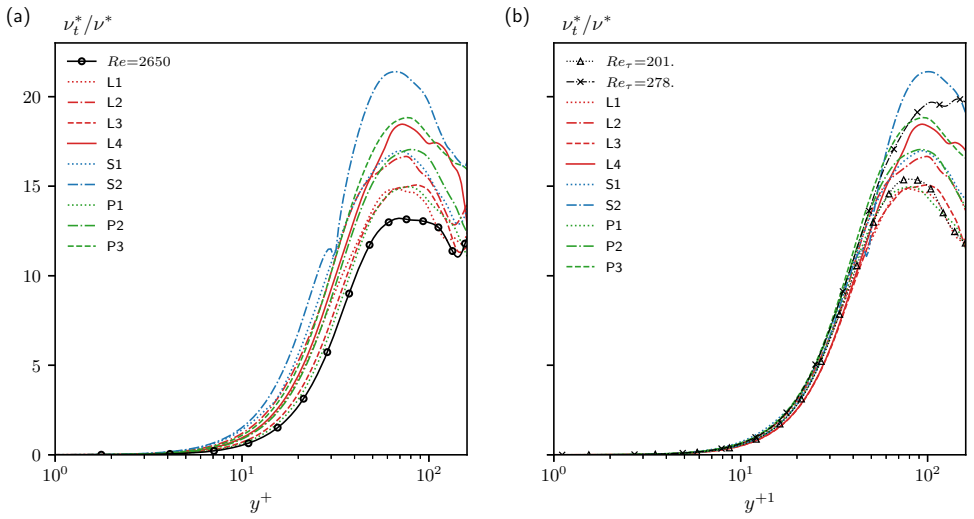

FIG. 2. Eddy viscosity profiles (ν_t) in standard inner scaling (a), and EPG scaling (b).

We now show that opposing body force influenced flows generally act like their EPG reference flows, except for the streamwise component of the turbulence which leads to interesting insight discussed in Sec. III C. To do this we inspect the eddy viscosity profiles (Fig. 2) defined as $\nu_t = \frac{-\overline{u_z' u_r'} Re}{d\bar{u}_z/dr}$, the root mean square (RMS) fluctuations (Fig. 3), and the Reynolds stress budgets (Figs. 4 and 5). We first note that the eddy viscosity profiles shown in Fig. 2(a) in conventional scaling increase significantly, which is inline with the conventional understanding that turbulence is enhanced as a result of the imposed body force. However, using the EPG scaling in Fig. 2(b), the eddy viscosity profiles in all flows collapse over each other in the near wall region (say, $y^{+1} < 50$); such a result suggests an interesting balance between mean shear and Reynolds shear stress, despite the additional body force. Whereas the relatively large spread in the core region simply reflects a low Reynolds number effect noting the differences between the two EPG reference flows shown. Later we demonstrate that this fact can be used to produce predictions of turbulence shear stress and skin friction. Similarity to the EPG flow is also clear in other turbulence statistics. Figure 3 shows the RMS fluctuations in each direction using the standard scaling [Figs. 3(a)–3(c)], and the alternative EPG scaling [Figs. 3(d)–3(f)]. In the usual scaling, and compared to their EFR reference case, the addition of the body force causes increased turbulence in all directions. There is a small increase of around 16% in the streamwise direction but a much larger increase of 70% in the wall normal and spanwise directions for the strongest case S2. The behavior is different in the EPG framework. There is very little change to the u_r' and u_θ' fluctuations and some of the small changes observed can be associated with the changes in their corresponding EPGs. On the other hand, u_z' reduces with increasing body force. This change is linked to changes in the streaks (and limited to this) and does not lead to significant changes in eddy viscosity as discussed above or other essential turbulence characteristics such as pressurestrain or vorticity to be discussed later. In general this means that the turbulence in body force opposed flows tends to behave in the same way as in their EPG flows, and hence can be thought of as acting according to an apparent Reynolds number (ARN) defined by that of its EPG flow.

The behavior of turbulence is further analyzed by comparing the budgets of the streamwise and wall-normal turbulent stresses in the conventional and EPG framework (Figs. 4 and 5). In the conventional framework, all turbulence activities increase with imposed body forces compared to their EFR reference flow. This includes the production, denoted I in the $\overline{u_z' u_z'}^+$ budget [Figs. 4(a)–4(c)] and the pressure strain, denoted IV in the $\overline{u_r' u_r'}^+$ budget [Figs. 5(a)–5(c)], acting as sources,

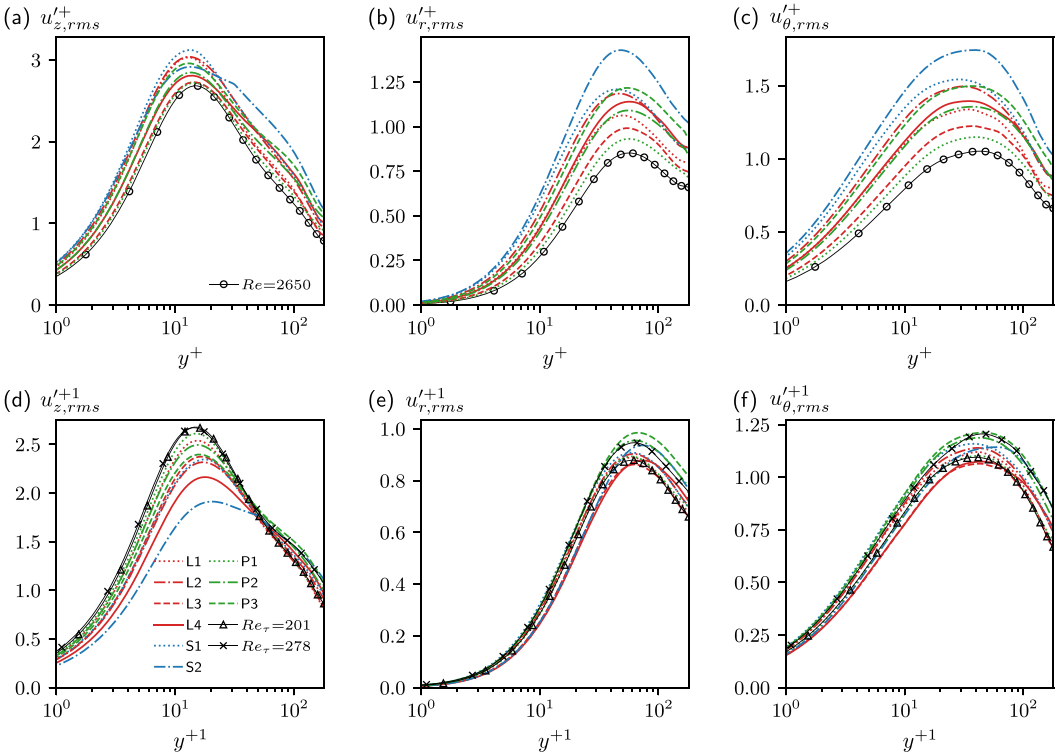

FIG. 3. Turbulent fluctuations in the streamwise, wall normal, and spanwise directions using the standard scaling (top row) and the EPG scaling (bottom row).

respectively, for each of them. In striking contrast, in the EPG framework, all the activities in the $\overline{u'_r u'_r}^{+1}$ budget [Figs. 5(d)–5(f)] including the pressure strain in the various body force influenced cases are little influenced by the body force, and all data agree well with each other. The maximum changes are less than 30% (only occurring in case $L4$) contrasting with the 2.9 times increase in the conventional framework. Similar conclusions can be drawn for the $\overline{u'_\theta u'_\theta}^{+1}$ budget (not shown). All the activities in the $\overline{u'_z u'_z}^{+1}$ budget [Figs. 4(d)–4(f)] except the pressure strain, however, reduce as the body force is imposed, which is consistent with u'^{+1}_z, shown in Fig. 3(d), and has no impact on other turbulence characteristics as discussed there. Such relative changes in the normal stresses lead to a more isotropic turbulence to be shown later.

C. Structures

The self-sustaining turbulence regeneration cycle, whereby turbulence is maintained by interactions between mean shear, streamwise streaks, and streamwise rolls, has been studied by numerous authors including Jiménez and Moin [34], Waleffe [35], Jiménez and Pinelli [33], and Kim [36]. The regeneration cycle can be seen as comprising a few distinct stages, that is, the formation and strengthening of streaks (leg one), breakdown of streaks and formation of streamwise-dependent structures (turbulence bursting, sweeps, ejections—leg two), and formation of streamwise vortices (leg three). Here we highlight some of the influences of body forces on these key structures, in particular with reference to the fact that u'_r and u'_θ are mostly related to bursting, while u'_z can have additional contribution from streaks. In Sec. III B we have shown that pressure strain, as well as u'_r and u'_θ fluctuations, remain unchanged in the EPG framework. These observations, and additionally

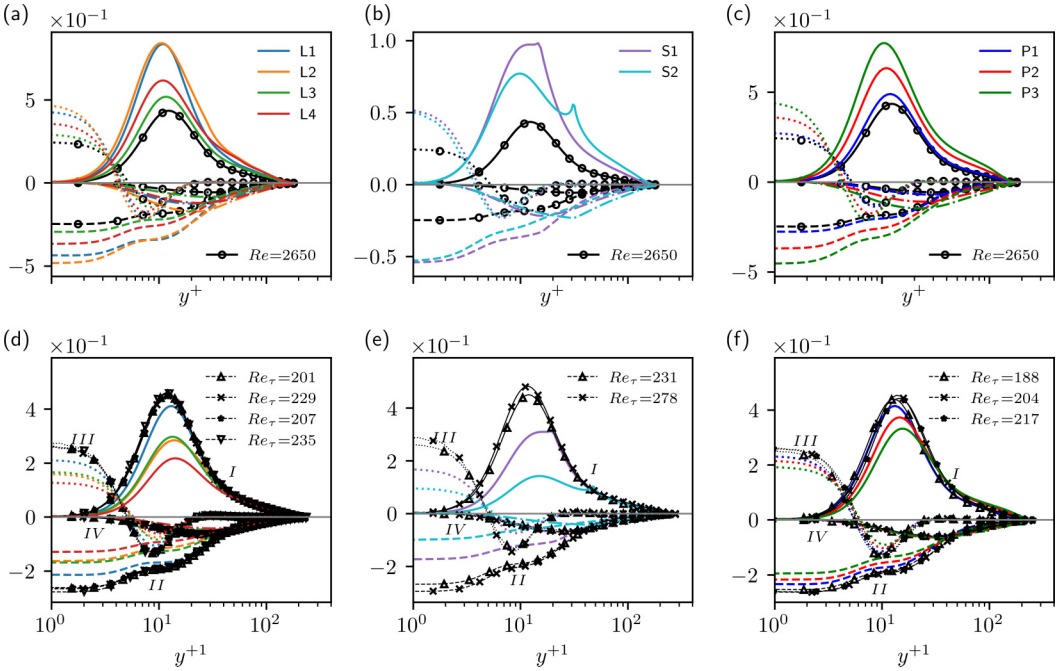

FIG. 4. Streamwise Reynolds stress budget terms using the standard scaling (top row), and the EPG scaling (bottom row) for linear (a), (d); step (b), (e); and physical (c), (f) cases. The terms shown are production (*I*), dissipation (*II*), viscous diffusion (*III*), and pressure strain (*IV*).

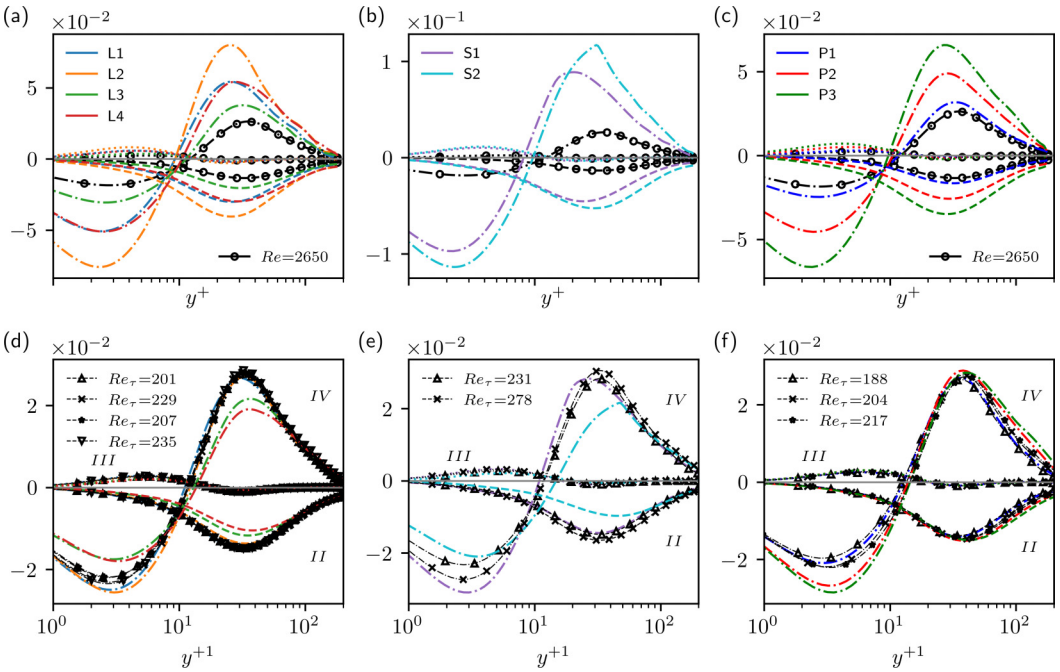

FIG. 5. Wall-normal Reynolds stress budget terms using the standard scaling (top row), and the EPG scaling (bottom row) for linear (a), (d); step (b), (e); and physical (c), (f) cases. The terms shown are dissipation (*II*), viscous diffusion (*III*), and pressure strain (*IV*).

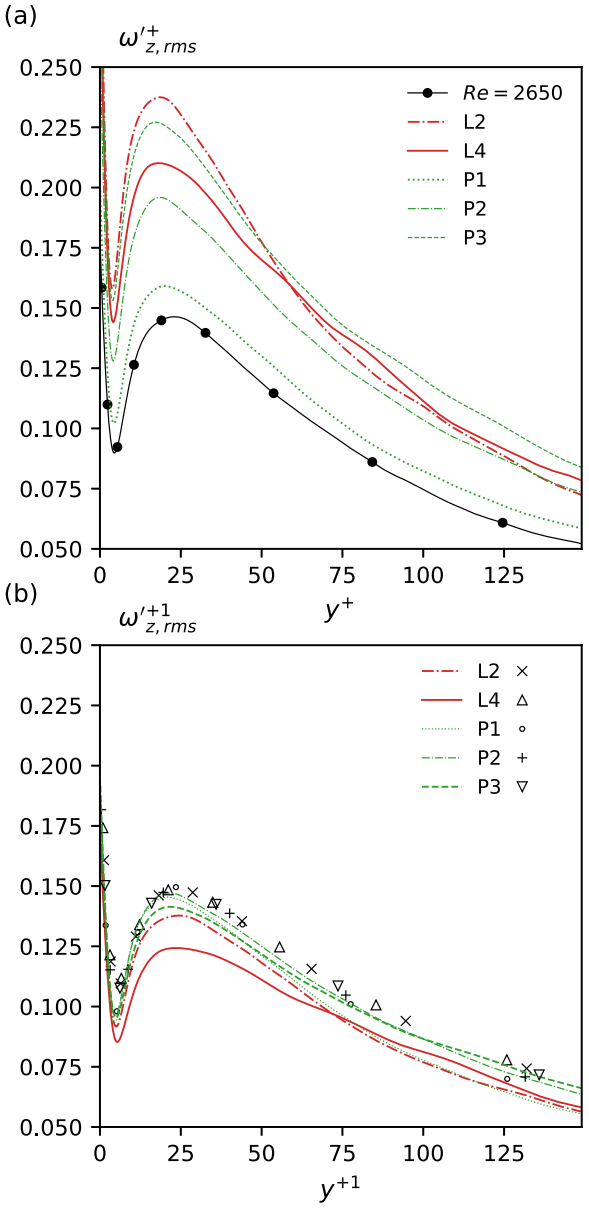

FIG. 6. Streamwise vorticity (a) uses the EFR reference flow, while (b) uses markers to represent each cases EPG reference flow.

the unchanging streamwise vorticity in Fig. 6(b), suggest that the second leg of the regeneration cycle is little affected by the body forces. We do expect changes to the first leg since we identified a weakening of the streaks as implied by the reduction in $u_z'^{+1}$ observed earlier. This can be visualized in Figs. 7(a) and 7(b), which show a stronger reduction in streaks amplitude in L4 than in its corresponding EPG flow. However the streak length in both aiding and opposing cases, indicated by the streamwise autocorrelations in Figs. 7(c) and 7(d), does not change. An exception is case L2a which is a strongly laminarized case and hence, the difference is likely due to low apparent Reynolds number effects. Overall, this is a remarkably similar conclusion to that of Jiménez [22]

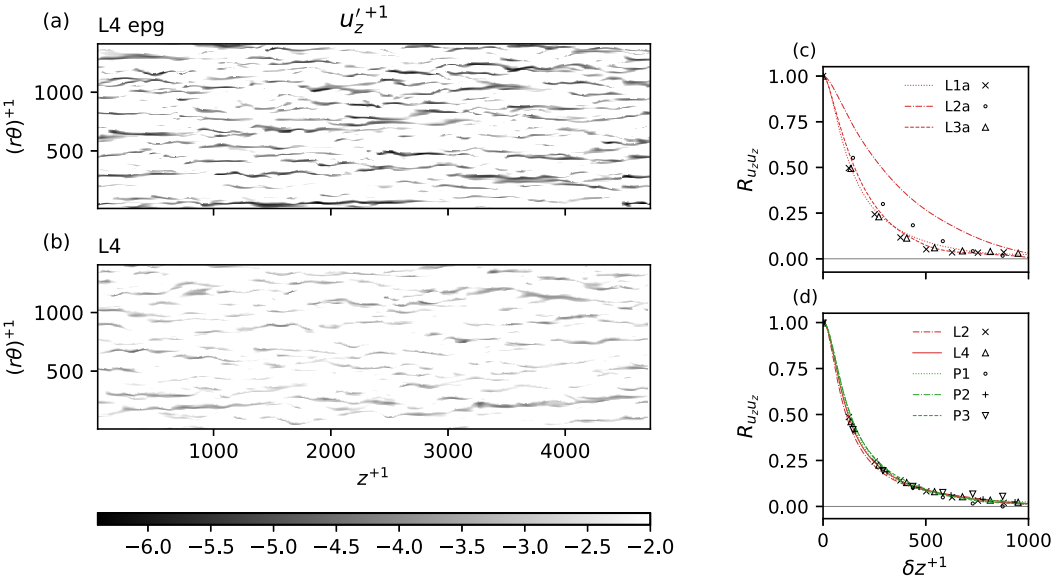

FIG. 7. Low speed streak visualizations for case L4 (a) and (b) and streamwise autocorrelations taken at $y^{+1} = 12$ with aided body force influenced cases (c) and opposed cases (d); markers represent the corresponding EPG reference cases.

who recently used numerical experiments to filter out large wavelengths causing severely shortened streaks while still maintaining the regeneration process in a channel flow. Jiménez [22] identified cases where the streamwise turbulence has the same length as the bursts while the burst structure is essentially indistinguishable from unmodified flows. Previously, Wu *et al.* [23] concluded that sublayer streaks appeared to be passive and are often simply observed as the rims of the indentation of the turbulence spots in a turbulent boundary layer.

Next we use quadrant analysis (Lu and Willmarth [37]) to identify how specific turbulence events are affected by body forces. Each quadrant is determined by the sign of u_z' and u_r', such that $Q1 : \{u_z' > 0, u_r' < 0\}$; $Q2 : \{u_z' < 0, u_r' < 0\}$; $Q3 : \{u_z' < 0, u_r' > 0\}$; and $Q4 : \{u_z' > 0, u_r' > 0\}$. The contribution to the shear stress is calculated by

$$\overline{u_z' u_r'}_Q = \lim_{T\to\infty} \frac{1}{T} \int_0^T (u_z' u_r') I(t)\, dt \tag{2}$$

and shown in the top row of Fig. 8. The frequency at which they happen is calculated using

$$N_Q = \lim_{T\to\infty} \frac{1}{T} \int_0^T I(t)\, dt \tag{3}$$

and shown in the bottom row of Fig. 8. The strength of events is determined by the value h such that $I(t) = 1$ if $|u_z' u_r'|_Q \geqslant h u_{z,rms}' u_{r,rms}'$ otherwise $I(t) = 0$. In this analysis we choose a moderate value of $h = 1$ in order to extract most events rather than only strong events. Clearly the dominant quadrants are the Q2 and Q4 quadrants, which correspond to ejections and sweep events. There is almost no increase in the frequencies of ejection and sweep events and very little change to their contribution to the turbulent shear stress compared to their EPG reference flows. Since ejection and sweep events are often interlinked with streak breakdown, this is another indication that the opposing body forces strongly alter the streaks and, as shown earlier, they do not alter the other aspects of the regeneration cycle, including streak breakdown.

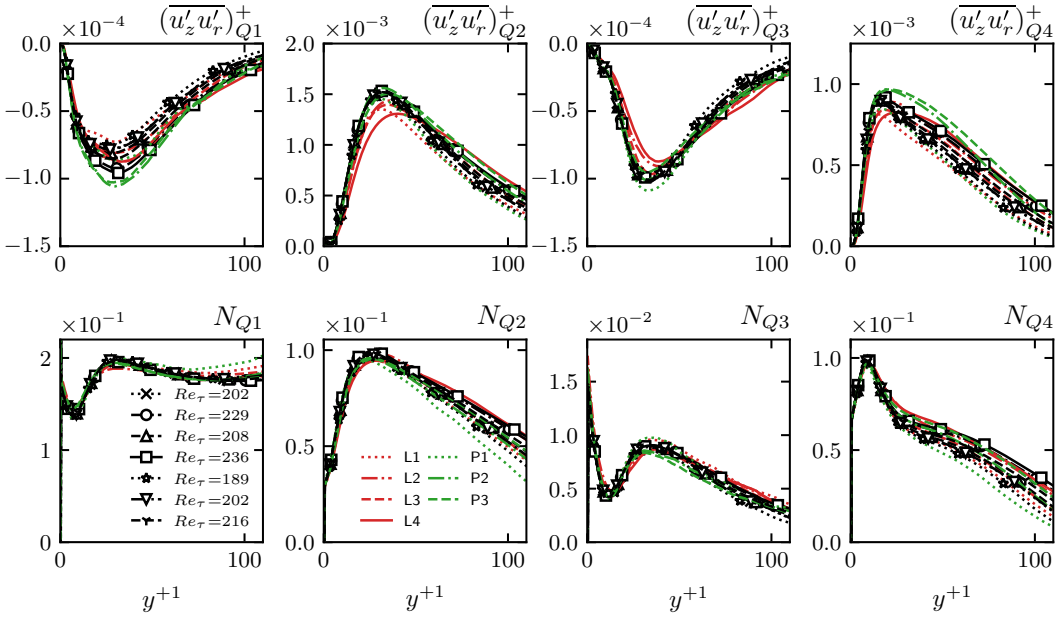

FIG. 8. Quadrant events with strength $h = 1$. Top row: contribution to the turbulent shear stress in each quadrant from such events. Bottom row: number of such events in each quadrant.

The changes in the regeneration cycle described above would imply changes in the anisotropy of the turbulence, noting the strong roles of the streaks here. This can be demonstrated using the anisotropic maps proposed by Lumley [38] based on second and third principle invariants, $II_a = Tr(b_{ij}b_{ji})$ and $III_a = Tr(b_{ij}^3)$, of the anisotropy tensor b_{ij} (Fig. 9). The opposing body force influenced flows [9(a) and 9(b)] with weakened streaks becoming more isotropic with increasing body force strength, which is to say that the anisotropy profiles move away from vertex A, representing one dimensional turbulence, toward vertices B and C, representing two and three dimensional turbulence, respectively. Whilst Fig. 9(c) shows increased anisotropy for the body force aided flows.

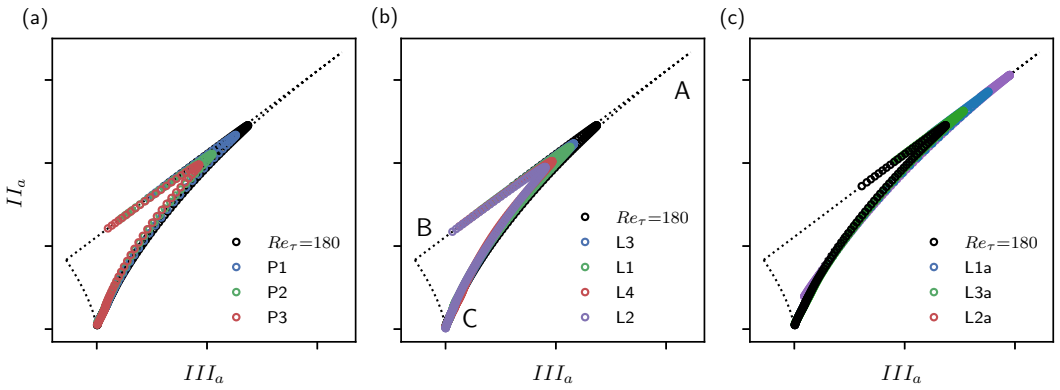

FIG. 9. Anisotropic maps where nodes A, B, and C represent 1one, two, and three dimensional turbulence, respectively.

We conclude that the key turbulence characteristics (e.g., eddy viscosity, vorticity, pressure strain, u_r', u_θ') are not significantly influenced by body forces under the EPG framework and the results from different flows correlate well. The turbulence streaks (and turbulence production and $u_z'^{+1}$) are, however, weakened by the body force, with little influence on other turbulence behaviors including mixing, for example.

D. Predictions

It is demonstrated in Sec. III B that some key turbulence quantities in such body force influenced flows can be scaled by the EPG parameters. Different from previous studies [25,28], we note that the streamwise turbulence and, as a result, the turbulent kinetic energy cannot be scaled in such a system. This is a natural consequence of the changes of the structures in such nonequilibrium flows discussed above. It however does not undermine the usefulness of this understanding. The ARN theory can be exploited following a method from He *et al.* [18] whereby the body force influenced RANS flow,

$$0 = -\frac{dp}{dx} + \frac{1}{r}\frac{\partial}{\partial r}\left[r\left(\frac{1}{Re}\frac{\partial \overline{u}_z}{\partial r} - \overline{u_z' u_r'}\right)\right] + f, \tag{4}$$

is split into its EPG flow,

$$0 = -\left(\frac{dp}{dx}\right)_p + \frac{1}{r}\frac{\partial}{\partial r}\left[r\left(\frac{1}{Re}\frac{\partial (\overline{u}_z)_p}{\partial r} - (\overline{u_z' u_r'})_p\right)\right], \tag{5}$$

where $(\frac{dp}{dx})_p = \frac{dp}{dx}$, and a perturbation flow due to the body force,

$$0 = \frac{1}{r}\frac{\partial}{\partial r}\left[r\left(\frac{1}{Re}\frac{\partial (\overline{u}_z)_b}{\partial r} - (\overline{u_z' u_r'})_b\right)\right] + f, \tag{6}$$

where $(\overline{u}_z)_b = \overline{u}_z - (\overline{u}_z)_p$ and $(\overline{u_z' u_r'})_b = \overline{u_z' u_r'} - (\overline{u_z' u_r'})_p$ are currently unknown. However, we know from Fig. 2(b) that the total flow and EPG flow have the same eddy viscosity, which means that the eddy viscosities for all the shear stresses in Eqs. (4)–(6) are the same, that is $\nu_t = \nu_{tb} = \nu_{tp}$. So applying the eddy viscosity hypothesis so that, $\overline{u_z' u_r'} = -\frac{\nu_t}{Re}\frac{\partial \overline{u}_z}{\partial r}$. Then the perturbation flow [Eq. (6)] can now be written as

$$0 = \frac{1}{r}\frac{\partial}{\partial r}\left[r\left(\frac{(1+\nu_{tp})}{Re}\frac{\partial (\overline{u}_z)_b}{\partial r}\right)\right] + f, \tag{7}$$

and solved for a given body force profile f. The total flow can then be obtained by summing the EPG and perturbation flow without directly solving body-force influenced flow Eq. 4.

The predictions of turbulence shear stress for the idealized cases and physical cases are shown in Figs. 10(a)–10(c). They are calculated from reference data for ν_t of the EPG flow and the given body force profiles. Despite the strong increase relative to their EFR reference case, and the nonequilibrium nature of the flows, the predictions are remarkably accurate. The physical cases also agree well with their equivalent turbulent shear stress profiles from You *et al.* [30], who used the boussinesq approximation, but still considered both the direct and indirect effects of buoyancy. This verifies the assumption that the structural effect is negligible in these flows.

Next we use the FIK expression introduced by Fukagata *et al.* [39] to determine different dynamical contributions to the skin friction,

$$C_f = \underbrace{\frac{16}{Re}}_{i} + \underbrace{16\int_0^1 2r^2(\overline{u_r' u_z'})_p\, dr}_{ii} + \underbrace{16\int_0^1 2r^2(\overline{u_r' u_z'})_b\, dr}_{iii} + \underbrace{16\int_0^1 (r^2-1)(f-F)r\, dr}_{iv}. \tag{8}$$

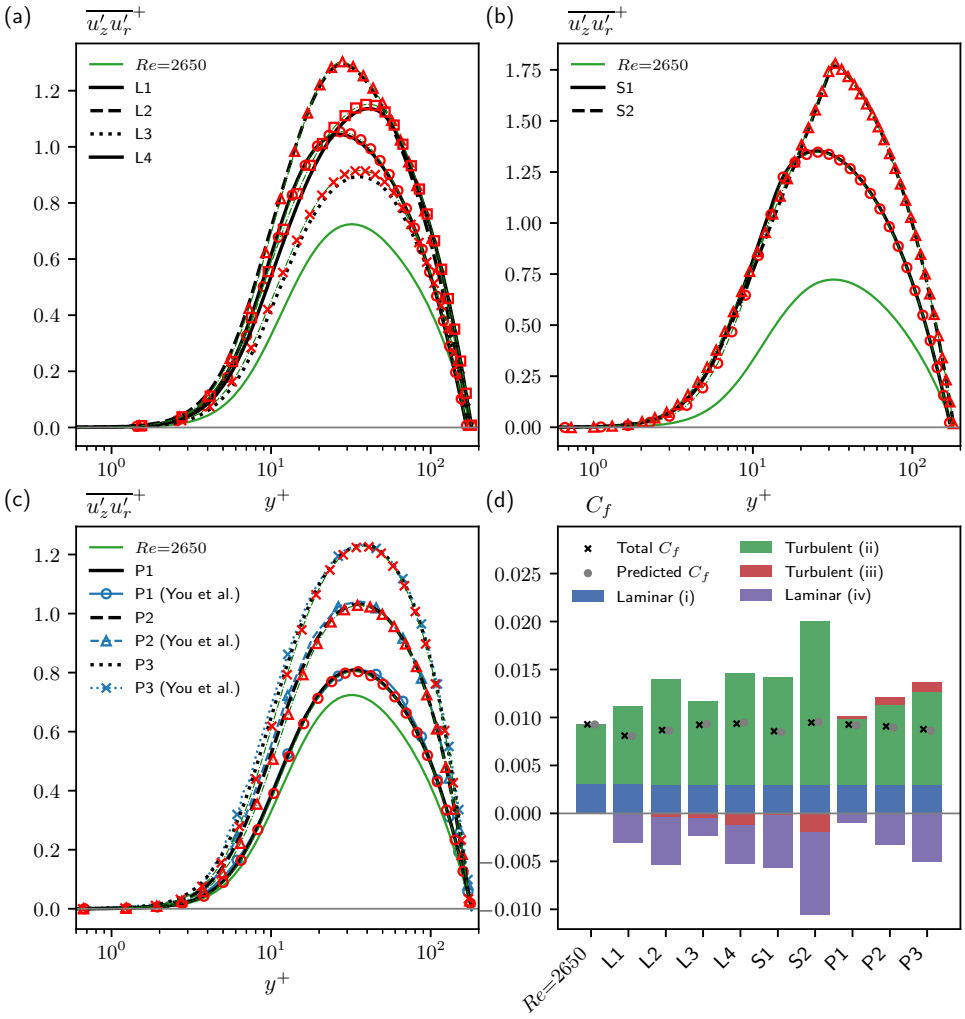

FIG. 10. Comparison of the apparent-Reynolds-number predictions (red markers) with DNS of the idealized linear and step change cases (a) and (b), and the physical cases (c). The latter also includes the equivalent profiles from You *et al.* [30] (blue markers). Subplot (d) shows the contributions to skin friction from various terms of the FIK decomposition defined in Eq. (8).

These include laminar contributions (i and iv) and turbulent contributions which are further split into the EPG and perturbation flows using the decomposition $\overline{u_z'u_r'} = (\overline{u_z'u_r'})_b + (\overline{u_z'u_r'})_p$. By using the predicted turbulent shear stress shown above, we obtain a prediction of C_f as seen in Fig. 10(d), agreeing very strongly with the actual DNS values.

IV. CONCLUSIONS

It is well established that turbulence may be significantly increased by a near-wall body force (such as buoyancy) opposing the flow. This statement is implicitly based on comparison under an equal flow rate basis. In contrast, we have shown here that applying a near-wall nonuniform body force while keeping the pressure gradient unchanged, that is in an equal pressure gradient basis, the key characteristics of turbulence, including the eddy viscosity and the transverse turbulence stresses,

remain largely unchanged. Thus, extending the framework of He *et al.* [18] from laminarization cases to explain body force induced turbulence enhancement. The streamwise turbulence stress reduces in this framework, which is traced to the weakened streaks or enhanced streaks for body force opposed and aided flows, respectively. This adds new information to recent discussion on the turbulence regeneration cycle, and supports the idea that the streaks may be very significantly modified without major influence to the overall turbulence regeneration. Turbulence enhancement in opposing body force flows in the conventional understanding is now associated with an increased apparent Reynolds number, defined by its EPG reference flow. By exploiting the unchanging eddy viscosity, usually difficult to predict quantities such as turbulent shear stress and skin friction, can be predicted well, simply from reference eddy viscosity and a given body force profile.

ACKNOWLEDGMENT

This work is funded by the University of Sheffield studentship and work was carried out using CHAPSim, which is maintained and supported by CCP NTH (EP/T026685/1).

[1] J. Kühnen, D. Scarselli, M. Schaner, and B. Hof, Relaminarization by steady modification of the streamwise velocity profile in a pipe, Flow, Turbul. Combust. **100**, 919 (2018).
[2] D. Scarselli, J. Kühnen, and B. Hof, Relaminarising pipe flow by wall movement, J. Fluid Mech. **867**, 934 (2019).
[3] J. Kühnen, B. Song, D. Scarselli, N. B. Budanur, M. Riedl, A. P. Willis, M. Avila, and B. Hof, Destabilizing turbulence in pipe flow, Nat. Phys. **14**, 386 (2018).
[4] J. Xu, S. Dong, M. R. Maxey, and G. E. Karniadakis, Turbulent drag reduction by constant near-wall forcing, J. Fluid Mech. **582**, 79 (2007).
[5] A. A. Arosemena, H. I. Andersson, and J. Solsvik, Turbulent channel flow of generalized Newtonian fluids at a low Reynolds number, J. Fluid Mech. **908**, A43 (2021).
[6] C. Henoch and J. Stace, Experimental investigation of a salt water turbulent boundary layer modified by an applied streamwise magnetohydrodynamic body force, Phys. Fluids **7**, 1371 (1995).
[7] J. D. Jackson, M. A. Cotton, and B. P. Axcell, Studies of mixed convection in vertical tubes, Int. J. Heat Fluid Flow **10**, 2 (1989).
[8] A. D. Carr, M. A. Connor, and H. O. Buhr, Velocity, temperature, and turbulence measurements in air for pipe flow with combined free and forced convection, J. Heat Transfer **95**, 445 (1973).
[9] B. P. Axcell and W. B. Hall, Mixed convection to air in a vertical pipe, in *Proceedings of the 6th International Heat Transfer Conference* (1978), Vol. 1, pp. 37–42.
[10] A. F. Polyakov and S. A. Shindin, Development of turbulent heat transfer over the length of vertical tubes in the presence of mixed air convection, Int. J. Heat Mass Transf. **31**, 987 (1988).
[11] V. A. Kurganov and A. G. Kaptilnyi, Velocity and enthalpy fields and eddy diffusivities in a heated supercritical fluid flow, Exp. Therm. Fluid Sci. **5**, 465 (1992).
[12] A. Steiner, On the reverse transition of a turbulent flow under the action of buoyancy forces, J. Fluid Mech. **47**, 503 (1971).
[13] J. P. Easby, The effect of buoyancy on flow and heat transfer for a gas passing down a vertical pipe at low turbulent reynolds numbers, Int. J. Heat Mass Transf. **21**, 791 (1978).
[14] A. M. Abdelmeguid and D. B. Spalding, Turbulent flow and heat transfer in pipes with buoyancy effects, J. Fluid Mech. **94**, 383 (1979).
[15] Y. Parlatan, N. E. Todreas, and M. J. Driscoll, Buoyancy and property variation effects in turbulent mixed convection of water in vertical tubes, J. Heat Transfer **118**, 381 (1996).
[16] B. S. Petukhov and A. F. Polyakov, Heat transfer in turbulent mixed convection (Hemisphere, New York, 1988).

[17] W. B. Hall and J. D. Jackson, Laminarization of a turbulent pipe flow by buoyancy forces, ASME-AMER SOC MECHANICAL ENG **91**, 66 (1969).
[18] S. He, K. He, and M. Seddighi, Laminarisation of flow at low Reynolds number due to streamwise body force, J. Fluid Mech. **809**, 31 (2016).
[19] F. J. G. García and P. F. Alvariño, On the analytic explanation of experiments where turbulence vanishes in pipe flow, J. Fluid Mech. **951**, A4 (2022).
[20] J. He, R. Tian, P. Jiang, and S. He, Turbulence in a heated pipe at supercritical pressure, J. Fluid Mech. **920**, A45 (2021).
[21] E. Marensi, S. He, and A. P. Willis, Suppression of turbulence and travelling waves in a vertical heated pipe, J. Fluid Mech. **919**, A17 (2021).
[22] J. Jiménez, The streaks of wall-bounded turbulence need not be long, J. Fluid Mech. **945**, R3 (2022).
[23] X. Wu, P. Moin, J. M. Wallace, J. Skarda, A. Lozano-Durán, and J.-P. Hickey, Transitional-turbulent spots and turbulent-turbulent spots in boundary layers, Proc. Natl. Acad. Sci. USA **114**, E5292 (2017).
[24] G. N. Coleman, J. Kim, and R. D. Moser, A numerical study of turbulent supersonic isothermal-wall channel flow, J. Fluid Mech. **305**, 159 (1995).
[25] P. G. Huang, G. N. Coleman, and P. Bradshaw, Compressible turbulent channel flows: DNS results and modelling, J. Fluid Mech. **305**, 185 (1995).
[26] E. R. Van Driest, Turbulent boundary layer in compressible fluids, J. Aeronaut. Sci **18**, 145 (1951).
[27] A. Trettel and J. Larsson, Mean velocity scaling for compressible wall turbulence with heat transfer, Phys. Fluids **28**, 026102 (2016).
[28] A. Patel, J. W. Peeters, B. J. Boersma, and R. Pecnik, Semi-local scaling and turbulence modulation in variable property turbulent channel flows, Phys. Fluids **27**, 095101 (2015).
[29] R. Pecnik and A. Patel, Scaling and modelling of turbulence in variable property channel flows, J. Fluid Mech. **823**, R1 (2017).
[30] J. You, J. Y. Yoo, and H. Choi, Direct numerical simulation of heated vertical air flows in fully developed turbulent mixed convection, Int. J. Heat Mass Transf. **46**, 1613 (2003).
[31] M. Seddighi-Moornani, Study of Turbulence and Wall Shear Stress in Unsteady Flow over Smooth and Rough Surfaces, Ph.D. Thesis, University of Aberdeen, 236 (2011).
[32] S. He and M. Seddighi, Turbulence in transient channel flow, J. Fluid Mech. **715**, 60 (2013).
[33] J. Jiménez and A. Pinelli, The autonomous cycle of near-wall turbulence, J. Fluid Mech. **389**, 335 (1999).
[34] J. Jiménez and P. Moin, The minimal flow unit in near-wall turbulence, J. Fluid Mech. **225**, 213 (1991).
[35] F. Waleffe, On a self-sustaining process in shear flows, Phys. Fluids **9**, 883 (1997).
[36] J. Kim, Physics and control of wall turbulence for drag reduction, Philos. Trans. R. Soc. A **369**, 1396 (2011).
[37] S. S. Lu and W. W. Willmarth, Measurements of the structure of the Reynolds stress in a turbulent boundary layer, J. Fluid Mech. **60**, 481 (1973).
[38] J. L. Lumley, Computational modeling of turbulent flows, *Advance in Applied Mechanics* (Elsevier, Amsterdam, Netherlands, 1979), Vol. 18, pp. 123–176.
[39] K. Fukagata, K. Iwamoto, and N. Kasagi, Contribution of Reynolds stress distribution to the skin friction in wall-bounded flows, Phys. Fluids **14**, L73 (2002).